A general peridynamics model for multiphase transport of non-Newtonian compressible fluids in porous media

Amit Katiyar[a]*, Shivam Agrawal[a]*, Hisanao Ouchi[a], Pablo Seleson[b], John T. Foster[a], Mukul M. Sharma[a]

[a]Department of Petroleum and Geosystems Engineering, The University of Texas at Austin, 200 E. Dean Keeton St., Stop C0300, Austin, TX 78712-1585, USA

[b]Oak Ridge National Laboratory, One Bethel Valley Road, P.O. Box 2008, MS 6211, Oak Ridge, TN 37831, USA

ABSTRACT

A general state-based peridynamics model is developed to simulate transport of fluids in an arbitrary heterogeneous porous medium. The generality encompasses modeling of multiphase, multi-component flow of non-Newtonian and compressible fluids, which is often encountered in but not limited to subsurface reservoirs. Peridynamic model is especially useful for solving non-local problems, such as crack propagation, since it does not assume spatial continuity of field variables. Thus, the formulation presented here, combined with peridynamics-based damage model, can be used to simulate hydraulic fracturing with complex fluids. To demonstrate its capability to simulate multi-phase flow in porous media, the derived model is verified against the analytical Buckley-Leverett solution for immiscible Newtonian two-phase flow. Further, the non-Newtonian two-phase fluid flow in porous media is verified by simulating the polymer flood process involving immiscible displacement of a Newtonian fluid by a non-Newtonian fluid against a generalized solution obtained by Wu, Pruess, and Witherspoon (1991). The non-local solutions are shown to be consistent with the corresponding local solutions in limiting cases. Moreover, mass conservation of all the phases is satisfied, irrespective of discretization and extent of non-locality.

1. Introduction

In a recent paper by Katiyar et al. (2014), a detailed mathematical formulation to obtain a governing peridynamic equation of transport of a single Newtonian fluid of small and constant compressibility through arbitrary heterogeneous porous media was developed. We use the adjective “peridynamic” here due to the similarity of our formulation to the peridynamic theory developed by Silling (2000) and Silling et al. (2007) within the field of solid mechanics. The peridynamic formulation was verified by simulating the transport of a fluid of uniform properties through a porous medium and comparing the results with those from a corresponding analytical model derived from the classical theory of flow in porous media. The peridynamic porous flow

* - equal author contribution

in fractured heterogeneous reservoirs. Reservoir hydrocarbons can be compressible, non-Newtonian and present in multiple phases. These fluids are also transported through the reservoirs for different applications such as hydraulic fracturing. Therefore, to simulate more realistic scenarios of fluid transport in heterogeneous porous media, the present work extends the previously developed model (Katiyar et al., 2014) to a more general peridynamic model of multiphase transport of a compressible, non-Newtonian fluid in porous media.

In Katiyar et al. (2014), motivations for developing a non-local peridynamic formulation for modeling porous flow were discussed. For completeness of this article, we summarize here some of the advantages. Fundamentally, the integral-equation based nonlocal peridynamic formulation remains valid even when discontinuities in the field variables appear in the domain. The peridynamic formulation also preserves both strong and weak discontinuities across domain boundaries without the need of special interface conditions as required by an equivalent classical model, for example an explicit flux continuity condition. Various complex systems in nature can elucidate diffusion processes due to local as well nonlocal potential differences. Nonlocal transport of fluids, observed in geological formations (Koch and Brady, 1988; Cortis and Berkowitz, 2004; Ganti et al., 2010), can be attributed to a reservoir's multi-scale heterogeneity in the form of material properties and/or natural fractures. The integral equation based non-local theory of peridynamics allows modeling of the transport effects of such spatial non-locality without explicitly resolving the multiscale heterogeneities. In addition to capturing this non-local transport, the fluid-flow formulation presented here provides a novel approach for simulating complex fluid-driven cracks when coupling it with the existing fracture mechanics model from peridynamic theory. Thus, it has practical applications in simulating hydraulic fracturing of unconventional hydrocarbon reservoirs.

The peridynamic theory was originally developed by Silling (2000) as a reformulation of the classical equation of motion for modeling elasticity and material failure in solid materials and structures. Bobaru and Duangpanya (2010) extended its application for simulating transient heat conduction in bodies with evolving discontinuities. Katiyar et al. (2014) developed and implemented a peridynamics theory for simulating fluid flow in porous media though limiting it only to the Newtonian fluids of constant and small compressibility. In the present work, through specializing the constitutive model of Seleson, Gunzburger, and Parks (2013), we relax such limitations to simulate compressibility and non-Newtonian behavior of fluids.

2. Mathematical Model

In this paper, we use both lower-case and upper-case letters for scalars, e.g. ρ, μ, t, A, V, lower case boldface letters and symbols for vectors, e.g., $\boldsymbol{x}$, $\boldsymbol{u}$, $\boldsymbol{\xi}$, upper-case bold face letters for second-order tensors in the local theory, e.g., $\boldsymbol{K}$ and blackboard letters for the corresponding second-order tensors in the non-local theory, e.g., $\mathbb{K}$. Borrowing from the mathematical notation of peridynamic mechanics, mathematical objects called peridynamic states have been introduced for convenience (Silling et al., 2007). In this formulation, we have used vector and scalar valued peridynamic states. Peridynamics states depend on position and time and operate on a vector connecting any two continuum material points. Depending on whether the mapped value of this operation is a scalar or vector, the state is called a scalar-state or a vector-state, respectively. To differentiate, peridynamic scalar states are denoted with underlined letters or symbols and peridynamic vector-states are denoted with underlined bold-faced letters. The mathematical definition of these peridynamic states is provided wherever they have been used in this work. In this article, we drop the explicit dependence on time, *t* to make the notation more concise.

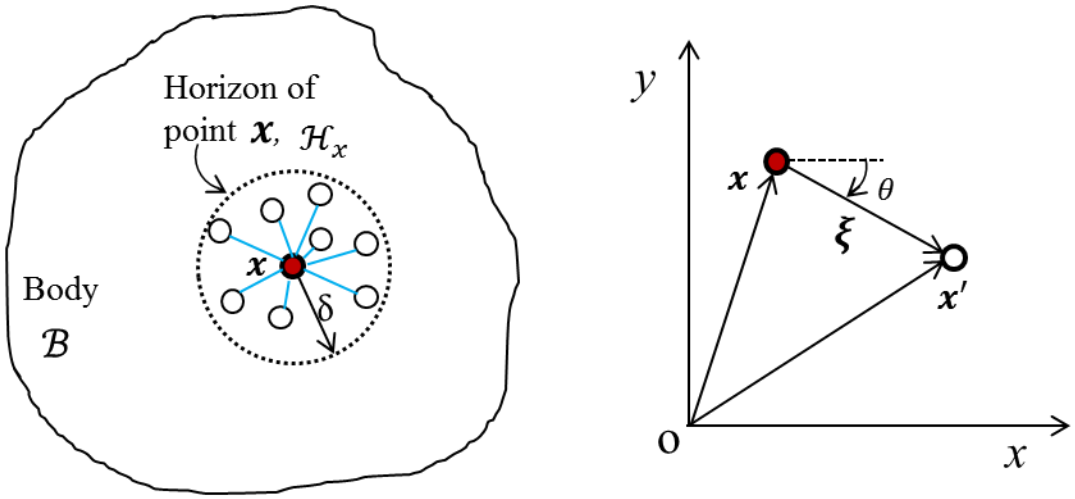

Figure 1. Left: schematic diagram of a peridynamic material point $\boldsymbol{x}$ and connected flow bonds in its horizon. Right: schematic of a flow bond between a material point $\boldsymbol{x}$ and its non-local neighboring material point $\boldsymbol{x}'$ in 2D.

2.1. State-Based Peridynamic Formulation of Single-phase Transport of Non-Newtonian and Compressible Fluid through Porous Media

The mass conservation equation for single-phase fluid flow in porous medium at position $\boldsymbol{x} \in \mathcal{B}$ and time t, using classical theory (Chen, Huan, and Ma, 2006), is

$$\frac{\partial}{\partial t}(\rho[\boldsymbol{x}]\emptyset[\boldsymbol{x}]) = -\nabla \cdot (\rho[\boldsymbol{x}]\boldsymbol{u}[\boldsymbol{x}]) + R[\boldsymbol{x}], \qquad \boldsymbol{u}[\boldsymbol{x}] = -\frac{1}{\mu[\boldsymbol{x}]}\boldsymbol{K}[\boldsymbol{x}]\nabla\Phi[\boldsymbol{x}] \tag{1}$$

where ρ is the fluid density, $\emptyset$ is the medium porosity, $\boldsymbol{u}$ is the volumetric flux, $\boldsymbol{K}$ is the material permeability tensor, μ is the fluid viscosity, Φ is the flow potential and R is the mass generation per unit bulk volume per unit time. In peridynamics, a material is assumed to be composed of material points of known density, and every material point interacts with all the neighboring material points inside a nonlocal region around it. Each interaction pair of a material point with its neighboring material point is referred as "bond".

In Katiyar et al. (2014), using variational arguments, a governing state-based peridynamic equation to simulate transport of single-phase flow of a liquid of small and constant compressibility through heterogeneous porous medium was developed. The resulting formulation is summarized in this sequel. Let a body in some reference configuration occupy a region $\mathcal{B}$ (Figure 1). The mass conservation equation for single-phase fluid flow in porous medium at position $\boldsymbol{x} \in \mathcal{B}$ and time t, using peridynamic theory, is

$$\frac{\partial}{\partial t}(\rho[\boldsymbol{x}]\emptyset[\boldsymbol{x}]) = \int_{\mathcal{H}_x} \left(\underline{Q}[\boldsymbol{x}]\langle\boldsymbol{\xi}\rangle - \underline{Q}[\boldsymbol{x}']\langle-\boldsymbol{\xi}\rangle\right) dV_{x'} + R[\boldsymbol{x}] \tag{2}$$

where $\mathcal{H}_x$ is the neighborhood of $\boldsymbol{x}$ referred as the "family of $\boldsymbol{x}$", which is a ball of radius δ referred to as the "horizon", $\underline{Q}$ is the peridynamic mass flow scalar state, $\boldsymbol{x}'$ is the position vector the neighboring points of $\boldsymbol{x}$ inside $\mathcal{H}_x$, $dV_{x'}$ is the differential volume of $\boldsymbol{x}'$, and $\underline{Q}[\boldsymbol{x}]\langle\boldsymbol{\xi}\rangle$ defined at position $\boldsymbol{x}$ operating on a "bond" $\boldsymbol{\xi} = \boldsymbol{x}' - \boldsymbol{x}$, maps the bond onto a net mass influx density in

that bond. In the local limit, the integral on the right-hand side of equation (2) replaces the divergence of the volumetric flux term from the equivalent classical theory.

$$-\nabla.(\rho[\boldsymbol{x}]\boldsymbol{u}[\boldsymbol{x}]) = \lim_{\mathcal{H}_x \to 0} \int_{\mathcal{H}_x} \left(\underline{Q}[\boldsymbol{x}]\langle \boldsymbol{\xi} \rangle - \underline{Q}[\boldsymbol{x}']\langle -\boldsymbol{\xi} \rangle \right) dV_{x'} \tag{3}$$

For simplicity, we make an assumption that the governing peridynamic equation for porous flow remains the same for multiple fluid phases and the extension of the model to simulate non-Newtonian and compressible fluid is modeled through the constitutive response.

2.1.1. Constitutive model

We propose a modified constitutive model of the form (Katiyar et al., 2014; Seleson, 2010)

$$\underline{Q}[\boldsymbol{x}]\langle \boldsymbol{\xi} \rangle = \frac{\gamma}{2} \underline{\omega}\langle \boldsymbol{\xi} \rangle \frac{\boldsymbol{\xi}.\widehat{\mathbb{K}}[\boldsymbol{x}].\boldsymbol{\xi}}{\|\boldsymbol{\xi}\|^4} (\Phi[\boldsymbol{x}'] - \Phi[\boldsymbol{x}]), \tag{4}$$

where γ is a scaling factor dependent on dimension d of the domain and the horizon size δ, $\underline{\omega}\langle \boldsymbol{\xi} \rangle$ is the influence function that provides an additional mechanism to modulate the nonlocal interactions (Seleson and Parks, 2011) and $\widehat{\mathbb{K}}$ is a symmetric constitutive tensor defined such that it ensures the convergence of the non-local model to the corresponding local model in the limit of the horizon going to zero. To determine $\widehat{\mathbb{K}}[\boldsymbol{x}]$, we seek to develop a relationship between $\widehat{\mathbb{K}}$ and the material properties (medium permeability $\boldsymbol{K}[\boldsymbol{x}]$, fluid density $\rho[\boldsymbol{x}]$ and fluid viscosity $\mu[\boldsymbol{x}]$), by imposing an equality between the nonlocal peridynamic model in the limit of horizon size $\delta \to 0$ and the corresponding well-established local model. Substituting equation (4) into the governing equation (2), we obtain

$$\frac{\partial}{\partial t}(\rho[\boldsymbol{x}]\emptyset[\boldsymbol{x}]) = \frac{\gamma}{2} \int_{\mathcal{H}_x} \underline{\omega}\langle \boldsymbol{\xi} \rangle \frac{\boldsymbol{\xi}.\left(\widehat{\mathbb{K}}[\boldsymbol{x}] + \widehat{\mathbb{K}}[\boldsymbol{x}']\right).\boldsymbol{\xi}}{\|\boldsymbol{\xi}\|^4} (\Phi[\boldsymbol{x}'] - \Phi[\boldsymbol{x}]) dV_{x'} + R[\boldsymbol{x}]. \tag{5}$$

For the purpose of establishing a connection to the local model, we momentarily assume continuously differentiable fields in $\mathbb{K}$ and Φ such that the following Taylor's expansions are admitted

$$\widehat{\mathbb{K}}[\boldsymbol{x}'] = \widehat{\mathbb{K}}[\boldsymbol{x}] + \boldsymbol{\xi} \cdot \nabla \widehat{\mathbb{K}}[\boldsymbol{x}] + \mathcal{O}(\|\boldsymbol{\xi}\|^2), \tag{6}$$

$$\Phi[x'] - \Phi[x] = (\boldsymbol{\xi} \cdot \nabla)\Phi[\boldsymbol{x}] + \frac{1}{2}(\boldsymbol{\xi} \cdot \nabla)(\boldsymbol{\xi} \cdot \nabla)\Phi[\boldsymbol{x}] + \mathcal{O}(\|\boldsymbol{\xi}\|^3), \tag{7}$$

Giving

$$\widehat{\mathbb{K}}[\boldsymbol{x}] + \widehat{\mathbb{K}}[\boldsymbol{x}'] = 2\widehat{\mathbb{K}}[\boldsymbol{x}] + \boldsymbol{\xi} \cdot \nabla \widehat{\mathbb{K}}[\boldsymbol{x}] + \mathcal{O}(\|\boldsymbol{\xi}\|^2). \tag{8}$$

Substituting equations (7) and (8) into equation (5), we obtain

$$\frac{\partial}{\partial t}(\rho[\boldsymbol{x}]\emptyset[\boldsymbol{x}]) = \gamma \int_{\mathcal{H}_x} \underline{\omega}\langle\boldsymbol{\xi}\rangle \frac{\boldsymbol{\xi}\cdot\left(\widehat{\mathbb{K}}[\boldsymbol{x}] + \frac{1}{2}\boldsymbol{\xi}\cdot\nabla\widehat{\mathbb{K}}[\boldsymbol{x}] + \mathcal{O}(\|\boldsymbol{\xi}\|^2)\right)\cdot\boldsymbol{\xi}}{\|\boldsymbol{\xi}\|^4} \times \left((\boldsymbol{\xi}\cdot\nabla)\Phi[\boldsymbol{x}] + \frac{1}{2}(\boldsymbol{\xi}\cdot\nabla)(\boldsymbol{\xi}\cdot\nabla)\Phi[\boldsymbol{x}] + \mathcal{O}(\|\boldsymbol{\xi}\|^3)\right) dV_{x'} + R[\boldsymbol{x}].$$

Collecting terms

$$\frac{\partial}{\partial t}(\rho[\boldsymbol{x}]\emptyset[\boldsymbol{x}]) =$$

$$= \gamma \int_{\mathcal{H}_x} \left(\underline{\omega}\langle\boldsymbol{\xi}\rangle \frac{\xi_i\xi_m\widehat{\mathbb{K}}_{mn}[\boldsymbol{x}]\xi_n\xi_j\frac{\partial}{\partial x_i x_j}\Phi[\boldsymbol{x}] + \xi_i\xi_m\frac{\partial\widehat{\mathbb{K}}_{mn}[\boldsymbol{x}]}{\partial x_i}\xi_n\xi_j\frac{\partial}{\partial x_j}\Phi[\boldsymbol{x}]}{2\|\boldsymbol{\xi}\|^4} \right) dV_{x'} + \mathcal{O}(\delta^2)$$

$$+ R[\boldsymbol{x}],$$

$$= \left[\gamma \int_{\mathcal{H}_x} \underline{\omega}\langle\boldsymbol{\xi}\rangle \frac{(\boldsymbol{\xi}\otimes\boldsymbol{\xi})\widehat{\mathbb{K}}[\boldsymbol{x}](\boldsymbol{\xi}\otimes\boldsymbol{\xi})}{2\|\boldsymbol{\xi}\|^4} dV_{x'}\right] : (\nabla\otimes\nabla)\Phi[\boldsymbol{x}]$$

$$+ \nabla.\left[\int_{\mathcal{H}_x} \gamma\underline{\omega}\langle\boldsymbol{\xi}\rangle \frac{(\boldsymbol{\xi}\otimes\boldsymbol{\xi})\widehat{\mathbb{K}}[\boldsymbol{x}](\boldsymbol{\xi}\otimes\boldsymbol{\xi})}{2\|\boldsymbol{\xi}\|^4} dV_{x'}\right].\nabla\Phi[\boldsymbol{x}] + \mathcal{O}(\delta^2) + R[\boldsymbol{x}],$$

$$= \left(\frac{\rho[\boldsymbol{x}]}{\mu[\boldsymbol{x}]}\boldsymbol{K}[\boldsymbol{x}]\right) : (\nabla\otimes\nabla)\Phi[\boldsymbol{x}] + \nabla.\left(\frac{\rho[\boldsymbol{x}]}{\mu[\boldsymbol{x}]}\boldsymbol{K}[\boldsymbol{x}]\right).\nabla\Phi[\boldsymbol{x}] + \mathcal{O}(\delta^2) + R[\boldsymbol{x}],$$

$$= \nabla\cdot\left(\frac{\rho[\boldsymbol{x}]}{\mu[\boldsymbol{x}]}\boldsymbol{K}[\boldsymbol{x}]\nabla\Phi[\mathrm{x}]\right) + \mathcal{O}(\delta^2) + R[\boldsymbol{x}], \tag{9}$$

where,

$$\frac{\rho[\boldsymbol{x}]}{\mu[\boldsymbol{x}]}\boldsymbol{K}[\boldsymbol{x}] = \int_{\mathcal{H}_x} \gamma\underline{\omega}\langle\boldsymbol{\xi}\rangle \frac{(\boldsymbol{\xi}\otimes\boldsymbol{\xi})\widehat{\mathbb{K}}[\boldsymbol{x}](\boldsymbol{\xi}\otimes\boldsymbol{\xi})}{2\|\boldsymbol{\xi}\|^4} dV_{x'}. \tag{10}$$

Taking $\delta \to 0$, we recover equation (1) from equation (9). By writing equation (10) in component form we establish a relationship between constitutive tensor $\widehat{\mathbb{K}}$ and material properties (medium permeability $\boldsymbol{K}[\boldsymbol{x}]$, fluid density $\rho[\boldsymbol{x}]$ and fluid viscosity $\mu[\boldsymbol{x}]$) with a judicious choice of scaling factor γ

$$\frac{\rho[\boldsymbol{x}]}{\mu[\boldsymbol{x}]}K_{ij}[\boldsymbol{x}] = \gamma\widehat{\mathbb{K}}_{nm}[\boldsymbol{x}] \int_{\mathcal{H}_x} \underline{\omega}\langle\boldsymbol{\xi}\rangle \frac{\xi_i\xi_n\xi_m\xi_j}{2\|\boldsymbol{\xi}\|^4} dV_{x'}. \tag{11}$$

Following Katiyar et al. (2014) and Seleson et al. (2013), it can be shown that the right hand side in equation (11) simplifies to

$$\frac{\rho[\boldsymbol{x}]}{\mu[\boldsymbol{x}]}K_{ij}[\boldsymbol{x}] = \gamma\big(\widehat{\mathbb{K}}_{ij}[\boldsymbol{x}] + \widehat{\mathbb{K}}_{ji}[\boldsymbol{x}] + \widehat{\mathbb{K}}_{kk}[\boldsymbol{x}]\delta_{ij}\big)\mathrm{I}_\delta^d \text{ where } \mathrm{I}_\delta^d = \frac{1}{3}\int_{\mathcal{H}_x} \underline{\omega}\langle\boldsymbol{\xi}\rangle \frac{\boldsymbol{\xi}_1^4}{2\|\boldsymbol{\xi}\|^4} dV_{x'}. \quad (12)$$

Choosing $\gamma = \frac{1}{2I_\delta^d}$, and using symmetry of $\widehat{\mathbb{K}}$, equation (11) becomes

$$\frac{\rho[\boldsymbol{x}]}{\mu[\boldsymbol{x}]}K_{ij}[\boldsymbol{x}] = \widehat{\mathbb{K}}_{ij}[\boldsymbol{x}] + \frac{1}{2}\widehat{\mathbb{K}}_{kk}[\boldsymbol{x}]\delta_{ij}. \quad (13)$$

Solving for $\widehat{\mathbb{K}}_{kk}$ for any dimension d,

$$\widehat{\mathbb{K}}_{kk}[\boldsymbol{x}] = \frac{2}{2+\mathrm{d}}K_{kk}[\boldsymbol{x}]\frac{\rho[\boldsymbol{x}]}{\mu[\boldsymbol{x}]}. \quad (14)$$

Substituting equation (14) into equation (13), we solve for $\widehat{\mathbb{K}}_{ij}$

$$\widehat{\mathbb{K}}_{ij}[\boldsymbol{x}] = \frac{\rho[\boldsymbol{x}]}{\mu[\boldsymbol{x}]}\Big(K_{ij}[\boldsymbol{x}] - \frac{1}{2+d}K_{kk}[\boldsymbol{x}]\delta_{ij}\Big). \quad (15)$$

Equation (15) relates the peridynamic constitutive tensor $\widehat{\mathbb{K}}$ with known material properties. In the next subsection, we derive the scaling factor based on the dimension of the problem and the choice of influence function.

2.1.2. Influence functions

2.1.2.1. $\underline{\boldsymbol{\omega}}\langle\boldsymbol{\xi}\rangle = \mathbf{1}$

This influence function gives the same weight to all the neighbors in the horizon. For two dimensions ($d = 2$), the horizon is a circle of radius δ and using polar coordinates, we have $\xi_1 = r\cos(\theta)$ and $\xi_2 = r\sin(\theta)$. Then, the scaling factor in two dimensions with $\underline{\omega}\langle\boldsymbol{\xi}\rangle = 1$ is

$$\gamma = \frac{3}{2}\left[\int_0^{2\pi}\int_0^{\delta}\frac{{\xi_1}^4}{2r^4}r\,dr\,d\theta\right]^{-1} = \frac{8}{\pi\delta^2}. \quad (16)$$

For three dimensions ($d = 3$), the horizon is a sphere of radius δ and using spherical coordinates, $\xi_1 = r\,sin(\varphi)\,cos(\theta)$, $\xi_2 = r\,sin(\varphi)\,sin(\theta)$ and $\xi_3 = r\,cos(\varphi)$. The scaling factor for three dimensions with $\underline{\omega}\langle\boldsymbol{\xi}\rangle = 1$ is

$$\gamma = \frac{3}{2}\left[\int_0^{2\pi}\int_0^{\pi}\int_0^{\delta}\frac{{\xi_1}^4}{2r^4}r^2\,sin(\varphi)\,dr\,d\varphi\,d\theta\right]^{-1} = \frac{45}{4\pi\delta^3}. \quad (17)$$

2.1.2.1. $\underline{\boldsymbol{\omega}}\langle\boldsymbol{\xi}\rangle = \mathbf{1} - \frac{\boldsymbol{r}}{\boldsymbol{\delta}}$

This influence function allows linearly varying contribution of the neighbors based on their proximity of the point of interest. Similar to equations (16) and (17), based on the dimension d we obtain following scaling factors for the constitutive model in equation (4)

$$\gamma = \begin{cases} \frac{3}{2}\left[\int_0^{2\pi}\int_0^{\delta}\left(1-\frac{\boldsymbol{r}}{\boldsymbol{\delta}}\right)\frac{\xi_1{}^4}{2r^4}r\,dr\,d\theta\right]^{-1} = \frac{24}{\pi\delta^2} \text{ for } d=2 \text{ and} \\ \frac{3}{2}\left[\int_0^{2\pi}\int_0^{\pi}\int_0^{\delta}\left(1-\frac{\boldsymbol{r}}{\boldsymbol{\delta}}\right)\frac{\xi_1{}^4}{2r^4}r^2\sin\varphi\,dr\,d\varphi\,d\theta\right]^{-1} = \frac{45}{\pi\delta^3} \text{ for } d=3. \end{cases} \tag{18}$$

Finally, for two dimensions $(d = 2)$, we substitute the scaling factor from equation (16) for $\underline{\omega}\langle\boldsymbol{\xi}\rangle = 1$ and the constitutive tensor from equation (15) into the original proposed constitutive model (4) to obtain

$$\underline{Q}[\boldsymbol{x}]\langle\boldsymbol{\xi}\rangle = \frac{\rho[\boldsymbol{x}]}{\mu[\boldsymbol{x}]}\frac{4}{\pi\delta^2}\frac{\boldsymbol{\xi}.\left(\boldsymbol{K}[\boldsymbol{x}]-\frac{1}{4}tr(\boldsymbol{K}[\boldsymbol{x}])\boldsymbol{I}\right).\boldsymbol{\xi}}{\|\boldsymbol{\xi}\|^4}(\Phi[\boldsymbol{x}']-\Phi[\boldsymbol{x}]), \tag{19}$$

$$-\underline{Q}[\boldsymbol{x}']\langle-\boldsymbol{\xi}\rangle = \frac{\rho[\boldsymbol{x}']}{\mu[\boldsymbol{x}']}\frac{4}{\pi\delta^2}\frac{\boldsymbol{\xi}.\left(\boldsymbol{K}[\boldsymbol{x}']-\frac{1}{4}tr(\boldsymbol{K}[\boldsymbol{x}'])\boldsymbol{I}\right).\boldsymbol{\xi}}{\|\boldsymbol{\xi}\|^4}(\Phi[\boldsymbol{x}']-\Phi[\boldsymbol{x}]), \tag{20}$$

$$\begin{aligned} &\frac{\partial}{\partial t}(\rho[\boldsymbol{x}]\emptyset[\boldsymbol{x}]) \\ &= \frac{4}{\pi\delta^2}\int_{\mathcal{H}_x}\frac{\boldsymbol{\xi}.\left(\frac{\rho[\boldsymbol{x}]}{\mu[\boldsymbol{x}]}\left(\boldsymbol{K}[\boldsymbol{x}]-\frac{1}{4}tr(\boldsymbol{K}[\boldsymbol{x}])\boldsymbol{I}\right)+\frac{\rho[\boldsymbol{x}']}{\mu[\boldsymbol{x}']}\left(\boldsymbol{K}[\boldsymbol{x}']-\frac{1}{4}tr(\boldsymbol{K}[\boldsymbol{x}'])\boldsymbol{I}\right)\right).\boldsymbol{\xi}}{\|\boldsymbol{\xi}\|^4}(\Phi[\boldsymbol{x}' \\ &-\Phi[\boldsymbol{x}])dA_{\boldsymbol{x}'}+R[\boldsymbol{x}]. \end{aligned} \tag{21}$$

For constant influence function $\underline{\omega}\langle\boldsymbol{\xi}\rangle = 1$, equation (20) is the governing peridynamic equation of single fluid porous flow in an arbitrary heterogeneous two dimensional medium. We simplify equation (20) for homogeneous and isotropic permeability, $\boldsymbol{K}[\boldsymbol{x}] = \boldsymbol{K}[\boldsymbol{x}'] = \kappa\boldsymbol{I}$ to obtain

$$\frac{\partial}{\partial t}(\rho[\boldsymbol{x}]\emptyset[\boldsymbol{x}]) = \frac{2}{\pi\delta^2}\int_{\mathcal{H}_x}\frac{\left(\frac{\rho[\boldsymbol{x}]}{\mu[\boldsymbol{x}]}+\frac{\rho[\boldsymbol{x}']}{\mu[\boldsymbol{x}']}\right)}{\|\boldsymbol{\xi}\|^2}(\Phi[\boldsymbol{x}']-\Phi[\boldsymbol{x}])dA_{x'}+R[\boldsymbol{x}] \tag{22}$$

In the next subsection, we report the extension of the single-phase model to multicomponent-multiphase transport of fluid through porous media.

2.2. State-Based Peridynamic Formulation of Multicomponent-multiphase Transport of Non-Newtonian and Compressible Fluid through Porous Media

Consider the permeable body $\mathcal{B}$ through which N_p phases consisting of N_c components flow. Neglecting diffusive mass transport, the mass conservation equation for a component α at any position $\boldsymbol{x} \in \mathcal{B}$ and time *t*, using the classical theory is

$$\frac{\partial}{\partial t}\left(\emptyset[\boldsymbol{x}]\sum_{\beta=1}^{N_p} S_\beta[\boldsymbol{x}]\rho_\beta[\boldsymbol{x}]w_{\alpha\beta}[\boldsymbol{x}]\right) = -\nabla.\left(\sum_{\beta=1}^{N_p}\rho_\beta[\boldsymbol{x}]\boldsymbol{u}_\beta[\boldsymbol{x}]w_{\alpha\beta}[\boldsymbol{x}]\right)+\sum_{\beta=1}^{N_p} w_{\alpha\beta}[\boldsymbol{x}]R_\beta[\boldsymbol{x}] \tag{23}$$

with constraints

$$\sum_{\beta=1}^{N_p} S_\beta[\boldsymbol{x}] = 1 \tag{24}$$

and

$$\sum_{\alpha=1}^{N_c} w_{\alpha\beta}[\boldsymbol{x}] = 1\,, \beta = 1,2,\dots\dots N_p \tag{25}$$

where S_β, ρ_β and R_β are the saturation, density and mass source of phase β respectively, $w_{\alpha\beta}$ is the mass fraction of component α in phase β and $\boldsymbol{u}_\beta$ is the phase volumetric flux obtained by extending Darcy's law for the physical properties of respective phases;

$$\boldsymbol{u}_\beta[\boldsymbol{x}] = -\boldsymbol{K}[\boldsymbol{x}]\frac{k_{r\beta}[\boldsymbol{x}]}{\mu_\beta[\boldsymbol{x}]}\nabla\Phi_\beta[\boldsymbol{x}]. \tag{26}$$

Here $k_{r\beta}$is the relative permeability of phase β, accounting for the reduction in permeability due to presence of the other phases, μ_β is the viscosity of phase β and Φ_β is the flow potential in phase β.

Analogous to equation (3), we can represent the divergence of the mass flux of component α in equation (23) by

$$-\nabla.\left(\sum_{\beta=1}^{N_p}\rho_\beta[\boldsymbol{x}]\boldsymbol{u}_\beta[\boldsymbol{x}]w_{\alpha\beta}[\boldsymbol{x}]\right) = \lim_{\mathcal{H}_x\to 0}\int_{\mathcal{H}_x}\sum_{\beta=1}^{N_p}\left(\underline{Q}_{\alpha\beta}[\boldsymbol{x}]\langle\boldsymbol{\xi}\rangle - \underline{Q}_{\alpha\beta}[\boldsymbol{x}']\langle-\boldsymbol{\xi}\rangle\right)dV_{x'} \tag{27}$$

We propose the following constitutive model to relate the mass flow state $\overline{Q}_{\alpha\beta}[\boldsymbol{x}]\langle\boldsymbol{\xi}\rangle$ to the flow potential of phase β

$$\underline{Q}_{\alpha\beta}[\boldsymbol{x}]\langle\boldsymbol{\xi}\rangle = \underline{Q}_\beta[\boldsymbol{x}]\langle\boldsymbol{\xi}\rangle\, w_{\alpha\beta}[\boldsymbol{x}] \tag{28}$$

where

$$\underline{Q}_{\beta}[\boldsymbol{x}]\langle\boldsymbol{\xi}\rangle = \frac{\gamma}{2}\underline{\omega}\langle\boldsymbol{\xi}\rangle\left(\frac{\boldsymbol{\xi}.\widehat{\mathbb{K}}_{\beta}[\boldsymbol{x}].\boldsymbol{\xi}}{\|\boldsymbol{\xi}\|^4}\right)\left(\Phi_{\beta}[\boldsymbol{x}'] - \Phi_{\beta}[\boldsymbol{x}]\right) \tag{29}$$

and the constitutive tensor $\widehat{\mathbb{K}}_{\beta}[\boldsymbol{x}]$ for respective phase is obtained in terms of material properties (medium permeability $\boldsymbol{K}[\boldsymbol{x}]$, relative phase permeability $k_{r\beta}[\boldsymbol{x}]$, phase density $\rho_{\beta}[\boldsymbol{x}]$ and phase viscosity $\mu_{\beta}[\boldsymbol{x}]$), by imposing an equality between the nonlocal peridynamic model in the limit of horizon size $\delta \to 0$ and the corresponding local model

$$\widehat{\mathbb{K}}_{\beta_{\boldsymbol{ij}}}[\boldsymbol{x}] = \rho_{\beta}[\boldsymbol{x}]\left(\frac{k_{r\beta}[\boldsymbol{x}]}{\mu_{\beta}[\boldsymbol{x}]}\right)\left(K_{ij}[\boldsymbol{x}] - \frac{1}{2+d}K_{kk}[\boldsymbol{x}]\delta_{ij}\right)$$

with constant scaling factor chosen the same as the single fluid formulation (Section 2.1). For example, in 2-dimensions and $\underline{\omega}\langle\boldsymbol{\xi}\rangle = 1$, the above proposed constitutive model in equation (28) with appropriate scaling factor (equation (16)) becomes

$$\underline{Q}_{\alpha\beta}[\boldsymbol{x}]\langle\boldsymbol{\xi}\rangle = \frac{4}{\pi\delta^2}\rho_{\beta}[\boldsymbol{x}]\left(\frac{k_{r\beta}[\boldsymbol{x}]}{\mu_{\beta}[\boldsymbol{x}]}\right)\frac{\boldsymbol{\xi}.\left(\boldsymbol{K}[\boldsymbol{x}] - \frac{1}{4}tr(\boldsymbol{K}[\boldsymbol{x}])\boldsymbol{I}\right).\boldsymbol{\xi}}{\|\boldsymbol{\xi}\|^4}\left(\Phi_{\beta}[\boldsymbol{x}'] - \Phi_{\beta}[\boldsymbol{x}]\right)w_{\alpha\beta}[\boldsymbol{x}]. \tag{30}$$

With a known constitutive model, the governing peridynamic equation for multicomponent-multiphase flow can be obtained from equations (23) and (27).

For modeling multiphase fluid flow in reservoirs, generally three types of models are considered: compositional models, black-oil models, and immiscible two-phase models (Coats et al, 1998). In a compositional model, the composition of the hydrocarbon components and water can strongly vary with space and time in different phases (aqueous, oleic, and gaseous) To track the phase compositions accurately, conservation equations for each of the components and appropriate equations of state are required, thereby making compositional models numerically expensive. A less complex alternative is the black-oil model which is detailed in the sequel.

2.2.1. Black-Oil Model

In a black-oil model, there are three phases namely, aqueous, oleic, and gaseous. A black-oil model is applicable when pressure is below the bubble point and mass can be transferred between the two hydrocarbon phases (Chen, Huan, and Ma, 2006). It is assumed that no mass is transferred between the aqueous and the other two phases. Gas solubility in oleic phase is assumed to depend only on pressure. Thus, all the hydrocarbons are represented by two pseudo hydrocarbon components, namely oil and gas.

In the following discussion, the two subscripts in the variables refer to components and phases respectively, unless otherwise stated. In the first subscript, index 1, 2, and 3 correspond to water, oil, and, gas components, respectively. In the second subscript, index 1, 2, and 3 correspond to aqueous, oleic and gaseous phases respectively. It is assumed that water can occur only in the aqueous phase, whereas oil and gas components can occur in either of the two hydrocarbon phases. Thus, mass fractions translate as

Aqueous phase: $w_{11} = 1, w_{21} = 0, w_{31} = 0$
Oleic phase: $w_{12} = 0, w_{32} = 1\text{-}w_{22}$
Gaseous phase: $w_{13} = 0, w_{23} = 1\text{-}w_{33}$

Neglecting capillary pressure (i.e., pressure difference between two immiscible phases due to surface and interfacial tension) between different phases, the LHS of equation (23) can be expanded as

$$\begin{aligned}\frac{\partial}{\partial t}\left(\emptyset[\boldsymbol{x}]\sum_{\beta=1}^{N_p} S_\beta[\boldsymbol{x}]\rho_\beta[\boldsymbol{x}]w_{\alpha\beta}[\boldsymbol{x}]\right) &= \left(\sum_{\beta=1}^{N_p} S_\beta[\boldsymbol{x}]\rho_\beta[\boldsymbol{x}]w_{\alpha\beta}[\boldsymbol{x}]\right)\emptyset[\boldsymbol{x}]c_r\frac{\partial p}{\partial t} \\ &+ \emptyset[\boldsymbol{x}]\left[\sum_{\beta=1}^{N_p}\left(\rho_\beta[\boldsymbol{x}]w_{\alpha\beta}[\boldsymbol{x}]\frac{\partial S_\beta[\boldsymbol{x}]}{\partial t} + \rho_\beta[\boldsymbol{x}]S_\beta[\boldsymbol{x}]\frac{\partial w_{\alpha\beta}[\boldsymbol{x}]}{\partial t}\right.\right. \\ &\left.\left. + S_\beta[\boldsymbol{x}]w_{\alpha\beta}[\boldsymbol{x}]\rho_\beta c_\beta\frac{\partial p_\beta}{\partial t}\right)\right]\end{aligned} \tag{31}$$

where c_r and c_j are the rock and phase compressibility respectively and are functions of pressure:

$$c_r(p) = \frac{1}{\emptyset}\frac{d\emptyset}{dp} \tag{32}$$

and

$$c_\beta(p_\beta) = \frac{1}{\rho_\beta}\frac{d\rho_\beta}{dp_\beta}. \tag{33}$$

In equations (32) and (33), it is assumed that porosity is a function of pressure and phase densities are functions of phase pressures alone, which is generally applicable for reservoir engineering applications. For the black-oil model, equation (23) simplified with equations (27) and (31) can be solved with appropriate initial and boundary conditions and known material properties. The black-oil model can further be simplified to the immiscible two-phase flow model.

2.2.2. Immiscible Two-Phase flow

Immiscible two-phase flow is a special case of black-oil model, in which there is no gaseous phase and no mass transfer takes place between phases. It is applicable when pressure is above the bubble point so that all the gas remains dissolved in oleic phase. The aqueous phase consists of only water component. Using the index notation described in the previous section, the above assumption translates into following mass fractions

$$w_{11} = 1, w_{21} = 0, w_{31} = 0, w_{12} = 0, w_{22} = w_{22}, w_{32} = 1 - w_{22}. \tag{34}$$

2.2.2.1. The Pressure Equation for Compressible Immiscible Two-Phase Flow

Adding the conservation equations of the gas and oil components gives one mass conservation equation for the oleic phase. From equations (23), (27), and (31), the conservation equation for each phase takes the following form:

$$\rho_\beta[\boldsymbol{x}]\left[\emptyset[\boldsymbol{x}]S_\beta[\boldsymbol{x}]\left(c_r\frac{\partial p}{\partial t}+c_\beta\frac{\partial p_\beta}{\partial t}\right)+\emptyset[\boldsymbol{x}]\frac{dS_\beta}{dt}\right] = \int_{\mathcal{H}_x}\left(\underline{Q}_\beta[\boldsymbol{x}]\langle\boldsymbol{\xi}\rangle-\underline{Q}_\beta[\boldsymbol{x}']\langle-\boldsymbol{\xi}\rangle\right)dV_{x'}+R_\beta[\boldsymbol{x}],\beta=1,2. \tag{35}$$

We divide equation (35) by $\rho_\beta[\boldsymbol{x}]$ and sum-up the resulting equation for both the phases to obtain

$$c_r\emptyset[\boldsymbol{x}]\frac{\partial p}{\partial t}+\emptyset[\boldsymbol{x}]\sum_{\beta=1}^{2}c_\beta S_\beta[\boldsymbol{x}]\frac{\partial p_\beta}{\partial t} = \sum_{\beta=1}^{2}\frac{1}{\rho_\beta[\boldsymbol{x}]}\int_{\mathcal{H}_x}\left(\underline{Q}_\beta[\boldsymbol{x}]\langle\boldsymbol{\xi}\rangle-\underline{Q}_\beta[\boldsymbol{x}']\langle-\boldsymbol{\xi}\rangle\right)dV_{x'}+q_t[\boldsymbol{x}] \tag{36}$$

where p is the total pressure, p_β is the phase pressure and $q_t[\boldsymbol{x}]=\left(\frac{R_1[\boldsymbol{x}]}{\rho_1[\boldsymbol{x}]}+\frac{R_2[\boldsymbol{x}]}{\rho_2[\boldsymbol{x}]}\right)$. Generally, total pressure is considered as the pressure in the aqueous phase and that the phase pressure in the oleic phase is obtained by accounting for capillary pressure. Relationships such as Brooks-Corey curves (Brooks and Corey, 1964) are used to calculate capillary pressure in terms of aqueous phase saturation.

$$p=p_1$$
$$p_2=p_1+p_{c,21}$$
$$p_{c,21}=f(S_w)$$

$p_{c,21}$ refers to the capillary pressure between phases 1 and 2.

In the process of simplifying the integral term in RHS of equation (36), we introduce the phase mobility $\lambda_\beta=k_{r\beta}/\mu_\beta$. For tractability of the equations, we further choose to simplify the integral term for a two-dimensional problem with homogeneous and isotropic permeability and $\underline{\omega}\langle\boldsymbol{\xi}\rangle=1$. We also define the pressure and gravitational head scalar-states respectively for each phase as:

$$\underline{P}_\beta[\boldsymbol{x}]\langle\boldsymbol{\xi}\rangle=p_\beta[\boldsymbol{x}']-p_\beta[\boldsymbol{x}],\qquad \underline{H}_\beta[\boldsymbol{x}]\langle\boldsymbol{\xi}\rangle=g\left(\rho_\beta[\boldsymbol{x}']z[\boldsymbol{x}']-\rho_\beta[\boldsymbol{x}]z[\boldsymbol{x}]\right) \tag{37}$$

where g is the acceleration due to gravity, and z is the height measured from a reference datum. Thus, the equation (36) becomes

$$c_r\emptyset[\boldsymbol{x}]\frac{\partial p}{\partial t}+\emptyset[\boldsymbol{x}]\sum_{\beta=1}^{2}c_\beta S_\beta[\boldsymbol{x}]\frac{\partial p_\beta}{\partial t} = \frac{2\kappa}{\pi\delta^2}\left[\int_{\mathcal{H}_x}\left(\frac{\rho_\beta[\boldsymbol{x}']}{\rho_\beta[\boldsymbol{x}]}\lambda_\beta[\boldsymbol{x}']+\lambda_\beta[\boldsymbol{x}]\right)\frac{\left(\underline{P}_\beta[\boldsymbol{x}]\langle\boldsymbol{\xi}\rangle+\underline{H}_\beta[\boldsymbol{x}]\langle\boldsymbol{\xi}\rangle\right)}{\|\boldsymbol{\xi}\|^2}dA_{x'}\right] + q_t[\boldsymbol{x}]. \tag{38}$$

Equation (38) is the pressure equation for compressible two-phase immiscible flow.

2.2.2.2. The Pressure Equation for Incompressible Immiscible Two-Phase Flow

Another simplifying assumption is to consider the rock and the two fluid phases incompressible, i.e. $c_r=c_1=c_2=0$. The pressure equation (38) then reduces to

$$\frac{2\kappa}{\pi\delta^2}\left[\int_{\mathcal{H}_x} M_{\rho\lambda_\beta}[\boldsymbol{x},\boldsymbol{x}']\frac{\left(\underline{P_\beta}[\boldsymbol{x}]\langle\boldsymbol{\xi}\rangle+\underline{H_\beta}[\boldsymbol{x}]\langle\boldsymbol{\xi}\rangle\right)}{\|\boldsymbol{\xi}\|^2}dA_{x'}\right]+q_t[\boldsymbol{x}]=0 \tag{39}$$

where

$$M_{\rho\lambda_\beta}[\boldsymbol{x},\boldsymbol{x}']=\left(\frac{\rho_\beta[\boldsymbol{x}']}{\rho_\beta[\boldsymbol{x}]}\lambda_\beta[\boldsymbol{x}']+\lambda_\beta[\boldsymbol{x}]\right)$$

For better decoupling of the pressure equation from the saturation equation, we follow Chavent and Jaffre (1986) and Aarnes, Gimse, and Lie (2007) and define a global pressure as $p^*=p_2-p_c$ that contains the saturation-dependent pressure terms p_c (complementary pressure) defined as

$$p_c=\int_1^{S_1} f_1(\zeta)\frac{\partial p_{c_{21}}(\zeta)}{\partial\zeta}d\zeta, f_1=\frac{M_{\rho\lambda_1}}{\left[M_{\rho\lambda_1}+M_{\rho\lambda_2}\right]} \tag{40}$$

$$\Rightarrow p_c[\boldsymbol{x}']-p_c[\boldsymbol{x}]=f_1\left(P_{c_{21}}[\boldsymbol{x}']-P_{c_{21}}[\boldsymbol{x}]\right)$$

$$\Rightarrow\left(M_{\rho\lambda_1}+M_{\rho\lambda_2}\right)\underline{p_c}(S_1)[\boldsymbol{x}]\langle\boldsymbol{\xi}\rangle=M_{\rho\lambda_1}\underline{P_{c_{21}}}(S_1)[\boldsymbol{x}]\langle\boldsymbol{\xi}\rangle$$

where $\underline{P_c}[\boldsymbol{x}]\langle\boldsymbol{\xi}\rangle=p_c[\boldsymbol{x}']-p_c[\boldsymbol{x}],\underline{P_{c_{21}}}[\boldsymbol{x}]\langle\boldsymbol{\xi}\rangle=P_{c_{21}}[\boldsymbol{x}']-P_{c_{21}}[\boldsymbol{x}]$. Thus, the pressure equation (39) simplifies to

$$\frac{4\kappa}{\pi\delta^2}\left[\int_{\mathcal{H}_x}\left(\left(M_{\rho\lambda_1}+M_{\rho\lambda_2}\right)\frac{\underline{P^*}[\boldsymbol{x}]\langle\boldsymbol{\xi}\rangle}{\|\boldsymbol{\xi}\|^2}+\frac{\left(M_{\rho\lambda_1}\underline{H_1}[\boldsymbol{x}]+M_{\rho\lambda_2}\underline{H_2}[\boldsymbol{x}]\right)\langle\boldsymbol{\xi}\rangle}{\|\boldsymbol{\xi}\|^2}\right)dA_{x'}\right]+q_t[\boldsymbol{x}] \tag{41}$$
$$=0$$

in only one pressure, p^* with $\underline{P^*}[\boldsymbol{x}]\langle\boldsymbol{\xi}\rangle=p^*[\boldsymbol{x}']-p^*[\boldsymbol{x}]$.

2.2.2.3. The Saturation Equation for Incompressible Immiscible Two-Phase Flow

Along with phase pressures, we also need to determine the phase saturations. For the two–phase flow case, the unknown saturations are of aqueous (S_1) and oleic (S_2) phases. However, the phase saturations are constrained by equation (23), so only one of the two phase-saturations needs to be determined and the common practice is to solve for S_1. From equation (35), the mass conservation equation for water component, with the incompressible rock and fluid assumption, is

$$\emptyset[\boldsymbol{x}]\frac{dS_1}{dt}=\frac{4\kappa}{\pi\delta^2}\int_{\mathcal{H}_x} M_{\rho\lambda_1}\frac{\left(\underline{P^*}[\boldsymbol{x}]\langle\boldsymbol{\xi}\rangle-\frac{M_{\rho\lambda_2}}{M_{\rho\lambda_1}}\underline{p_c}[\boldsymbol{x}]\langle\boldsymbol{\xi}\rangle\right)+\underline{H_1}[\boldsymbol{x}]\langle\boldsymbol{\xi}\rangle}{\|\boldsymbol{\xi}\|^2}dA_{x'}+R_1[\boldsymbol{x}] \tag{42}$$

which serves as the saturation equation for incompressible immiscible two-phase flow. The pressure equation (41) is solved with the saturation dependent properties and the saturation equation is solved with the global pressure obtained from the pressure equation (41).

3. Model Verification

We verify the peridynamics multiphase flow model by solving the immiscible displacement of one fluid by another. One-dimensional flow is solved in a uniform horizontal reservoir with a fluid injection source at one end and a production sink at the other. For simplicity, it is assumed that the rate of fluid injection and the rate of fluid production at the respective ends are the same.

The model presented here can simulate complex fluids since it accounts for compressible and non-Newtonian behavior. In this section, two verification problems are considered – one in which Newtonian water displaces Newtonian oil and the other in which a non-Newtonian polymer solution displaces Newtonian oil. In the petroleum engineering community, these displacement processes are known as 'water flood' and 'polymer flood' respectively. The fluids are assumed to be slightly compressible in both the problems.

3.1. Problem 1: Immiscible displacement of a Newtonian fluid (oil) by another Newtonian fluid (water) ─ Water flood

A schematic of this verification problem is shown in Figure 2. The model parameters are summarized in Table 1. A Brooks-Corey relationship (Brooks and Corey, 1964) is assumed for calculating relative permeability of the two phases:

$$k_{rw}(S_w) = k_{rw}^0 * (S_{wD})^{N_w} \tag{43}$$

$$k_{ro}(S_w) = k_{ro}^0 * (1 - S_{wD})^{N_o} \tag{44}$$

where S_w is water saturation, $k_{rw}{}^0$ and $k_{ro}{}^0$ are end-point relative permeabilities, and N_w and N_o are relative permeability exponents of aqueous and oleic phase respectively. S_{wD} is dimensionless water saturation and is defined as:

$$S_{wD} = \frac{S_w - S_{wr}}{1 - S_{or} - S_{wr}}. \tag{45}$$

where S_{wr} and S_{or} are residual saturations of water and oil respectively.

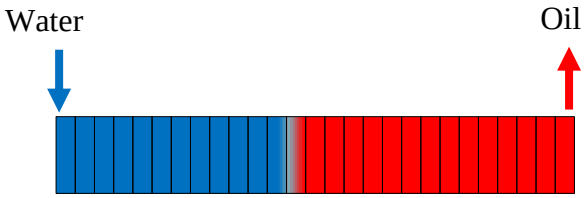

Figure 2. Schematic of water flood process. Cooler colors represent higher saturations of water, whereas warmer colors represent higher saturations of oil (scale in the width direction is highly exaggerated)

Table 1. Simulation parameters for Problem 1

Length of domain *(L_x)*	200 m
Porosity *(φ)*	30%
Permeability *(κ)*	100 mD

Initial pressure *(P_{ini})*	20 MPa
Initial water saturation *($S_{w,\,ini}$)*	0.0
Residual saturations of both fluids *(S_{wr} and S_{or})*	0.0
End-point relative permeability for both fluids *(k_r)*	1.0
Relative permeability exponents for both fluids *(N)*	2
Density of both fluids *(ρ_w and ρ_o)*	1 kg/m^3
Viscosity of both fluids *(μ_w and μ_o)*	1 cP
Rate of injection and production *(Q)*	4e-5 kg/s

3.1.1. Numerical discretization

The computational domain is discretized into uniform grid cells of size $\Delta x = \Delta y = \Delta z = L_x/n_x$, where L_x is the length of the domain and n_x is the number of grid cells in x-direction. Since our objective is to simulate 1-D flow, there is just one cell in y- and z- directions. One computational node is assumed at the center of each grid cell and is assigned a volume equivalent to that of one cell, $(\Delta x)^3$.

3.1.2. Analytical local solution

The mobility ratio for an immiscible displacement process is defined as:

$$M = \frac{M_w}{M_o} = \frac{k_{rw}/\mu_w}{k_{ro}/\mu_o} \tag{46}$$

where M_w and M_o are the mobilities of aqueous and oleic phases respectively.

For $M \leq 1$, a piston-like displacement occurs which is characterized by the formation of a shock-front. As in-situ fluid is displaced, it moves from injector well towards the producer well. Before the shock-front reaches the producer well, only in-situ fluid is produced. When it has reached the producer well, the displacing fluid breaks through and both fluids are produced thereafter.

Neglecting gravity and capillary pressure between the aqueous and oleic phases, the analytical local solution can be obtained by using the fractional flow theory established by Buckley and Leverett (1941). For completeness, the steps for finding the analytical local solution have been summarized here.

a) Fractional flow of water phase is given as:

$$f_w(S_w) = \frac{q_w}{q_w + q_o} = \frac{k_{rw}(S_w)/\mu_w}{k_{rw}(S_w)/\mu_w + k_{ro}(S_w)/\mu_o} \tag{47}$$

b) The water saturation at the shock front (S_{wf}) is obtained by solving the following equation:

$$\left.\frac{\partial f_w}{\partial S_w}\right|_{S_{wf}} = \frac{f_{wf}}{S_{wf} - S_{w,ini}} \tag{48}$$

c) The position of the shock front is determined as:

$$x_D = \left.\frac{\partial f_w}{\partial S_w}\right|_{S_{wf}} * t_D. \tag{49}$$

d) The reservoir behind the shock front is swept by water, thereby increasing water saturation in that region. For all water saturations greater than the shock front water saturation obtained in equation (48), $\left.\frac{\partial f_w}{\partial S_w}\right|_{S_w}$ is calculated by differentiating equation (47).

e) At a given dimensionless time (t_D), the dimensionless position (x_D) of each water saturation greater than the shock front water saturation can be calculated as:

$$x_D = \left.\frac{\partial f_w}{\partial S_w}\right|_{S_w} * t_D \tag{50}$$

f) The reservoir ahead of the shock front has not been swept by water yet. Thus, in the region ahead of the shock-front:

$$S_w = S_{w,ini} \tag{51}$$

3.1.3. Peridynamic solution

Figure 3 shows the analytical local and peridynamic solutions to the classical Buckley Leverett problem for *M=1*. Dimensionless water saturation *(S_{wD})* is plotted against dimensionless distance from the injector well *(x_D)* at a dimensionless time *(t_D)*. These parameters are defined as:

$$x_D = \frac{x}{L_x} \tag{52}$$

$$t_D = \frac{Q * t}{\rho * PV} \tag{53}$$

where Q is the injection rate (kg/s), ρ is density of injected fluid (kg/m^3), and PV is the pore volume injected (m^3) *(= Porosity * domain volume).*

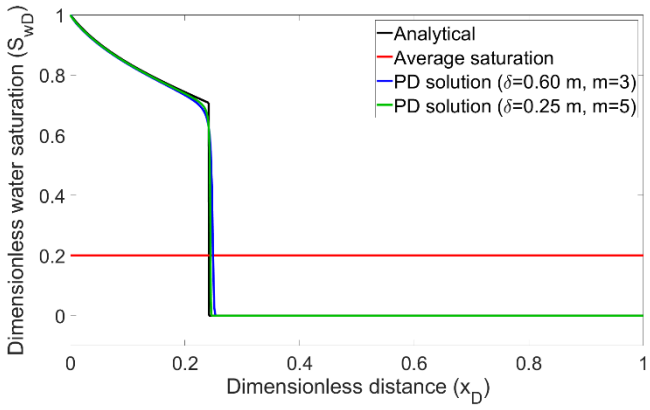

(a)

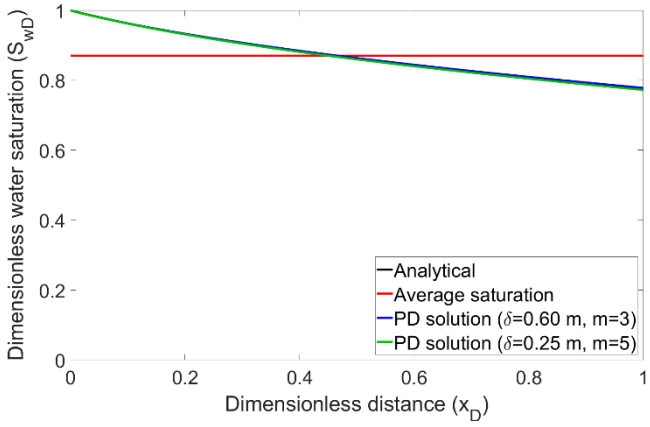

(b)

Figure 3. Analytical local and peridynamic (PD) saturation profiles for water flood problem. (a): before breakthrough (at $t_D = 0.2$). (b): after breakthrough (at $t_D = 1.2$). *m* is the number of non-local neighbors for each cell (described in more detail in Section 3.1.4)

The sharp discontinuity in analytical local solution is the shock-front described above. Except for the smearing of the shock-front in Figure 3 (a), the peridynamic solution matches water saturation from the analytical local solution very well, both behind and ahead of the shock-front, and both before and after the breakthrough. It should be noted that the smearing of the shock-front is a characteristic of the non-local contributions to diffusion terms in equations (1) and (23). These non-local contributions become smaller as the horizon size is shrunk (Bobaru and Ha 2011). Using the curves shown in these figures, a convergence study for the waterflood problem is discussed in the next sub-section.

3.1.4. Convergence study

Peridynamics is a non-local formulation and accounts for interactions from all its neighboring nodes within a characteristic length scale, called horizon *(δ)*. If a 1-D domain is discretized into

uniform cell size of length Δx, the number of non-local neighbors to each cell is *m (=δ/Δx)* in each direction.

The non-local peridynamic solution converges to the local solution in the limit of δ going to zero and *m* being infinitely large simultaneously. Such a convergence study is referred to as δ-*m* convergence study (Bobaru et al, 2009). Please note that this study is different from the *m*-convergence study taken up in Katiyar et al. (2014). The objective in that work was to find an optimum choice for both δ and *m* by varying *m* for different values of δ. The objective here is to show that the local solution can be recovered from non-local solution in the limiting case.

Four cases were considered with successively smaller δ and larger *m*. The values for these parameters are given in Table 2.

Table 2. Horizon size *(δ)* and number of non-local neighbors *(m)* for the three cases

Case	Horizon size *(δ)*	Number of non-local neighbors *(m)*
1	0.80 m	2
2	0.60 m	3
3	0.40 m	4
4	0.25 m	5

Figure 4 demonstrates the convergence of non-local solution towards the local solution by plotting relative differences for the four cases. With reference to Figure 3, relative difference is defined as:

$$\text{Relative difference} = \frac{\sum_x \left| S_{w,analytical} - S_{w,numerical} \right|}{A_{analytical}} * 100 \tag{54}$$

where $A_{analytical}$ is the area under the analytical local curves in Figure 3.

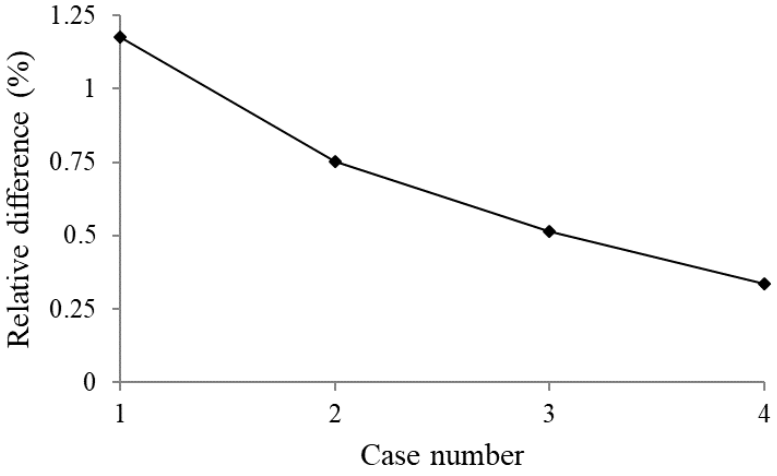

Figure 4. Relative difference in water saturation profile as horizon size *(δ)* decreases and number of non-local neighbors *(m)* increases simultaneously as shown in Table 2.

A higher number of non-local neighbors requires higher computational resources owing to denser coefficient matrices. Thus, unless otherwise stated, we use *m=3* in the subsequent simulations to get a reasonably accurate non-local solution, while retaining a low computational cost. The choice of this value of *m* comes from our experience gained so far with peridynamic simulations.

3.2. Problem 2: Immiscible displacement of a Newtonian fluid (oil) by a non-Newtonian fluid (polymer) – Polymer flood

In this verification problem, Newtonian oil is displaced by a shear-thinning polymer solution and a schematic is shown in Figure 5. Polymer solution is injected at different rates to study the effect of injection rate on oil recovery. Except for the viscosity of the displacing fluid and the injection and production rates, the rest of the parameters remain the same as in verification problem 1 and are summarized in Table 3. Power law relationship is assumed between polymer viscosity and shear rate:

$$\mu_p = H * (\dot{\gamma})^{n-1} \tag{55}$$

where μ_p is the polymer viscosity, $\dot{\gamma}$ is the shear rate, *H* is the intrinsic viscosity, and *n* is the power law exponent.

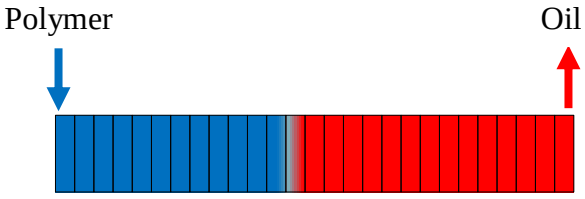

Figure 5. Schematic of polymer flood process. Cooler colors represent higher saturations of polymer, whereas warmer colors represent higher saturations of oil (scale in vertical direction is highly exaggerated)

Table 3. Simulation parameters for Problem 2

Length of domain *(L_x)*	200 m
Porosity *(φ)*	30%
Permeability *(κ)*	100 mD
Initial pressure *(P_{ini})*	20 MPa
Initial polymer saturation *($S_{w,\,ini}$)*	0.0
Residual saturations of both fluids *(S_r)*	0.0
End-point relative permeability for both fluids *(k_r)*	1.0
Relative permeability exponents for both fluids *(N)*	2

Density of both fluids *(ρ_p and ρ_o)*	1 kg/m^3
Viscosity of oil *(μ_o)*	1 cP
Intrinsic viscosity of polymer *(H)*	1 cP
Power law exponent *(n)*	0.5
Rate of injection and production *(Q)*	4e-5 kg/s in fast injection rate 4e-6 kg/s in slow injection rate

3.2.1. Analytical local solution

Following the incompressibility assumption, total flow of both the fluids at any cross-section should remain constant with time and should be equal to the injection rate:

$$u(t) = u_{injection} = u_{oil} + u_{polymer} \tag{56}$$

Using Darcy's law, flow rates of oil and polymer solution can be written as:

$$u_{oil} = -\kappa \frac{k_{r,oil}}{\mu_{oil}} \frac{\partial P}{\partial x} \tag{57}$$

$$u_{polymer} = -\kappa \frac{k_{r,polymer}}{\mu_{polymer}} \frac{\partial P}{\partial x} \tag{58}$$

We used the relationship for equivalent non-Newtonian viscosity derived by Wu et al. (1991). Combining the above three equations with the constitutive relations (43), (44), and (55), they plotted the pressure gradients as a function of non-Newtonian fluid saturation (polymer saturation) for different injection rates.

Figure 6 demonstrates that at faster injection rates of the polymer, the pressure gradients are higher for any given polymer saturation. This leads to higher shear rates, which in turn result in lower viscosity of the shear thinning polymer. From Buckley-Leverett analysis, it is known that lower viscosity of the displacing fluid leads to reduced sweep efficiency and hence less oil recovery. This idea is used to verify the peridynamic solution for immiscible displacement by a non-Newtonian fluid.

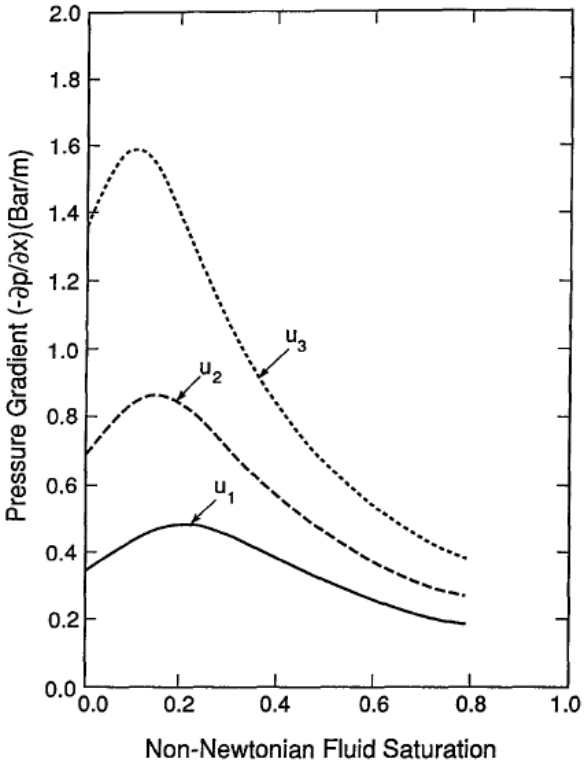

Figure 6. Pressure gradient as a function of non-Newtonian fluid (polymer solution) saturation in a polymer flood (Wu et al., 1991). In that study, it is assumed that $u_3 > u_2 > u_1$.

3.2.2. Peridynamic solution

Figure 7 shows the saturation profiles for two different injection rates before the displacing polymer solution breaks through at the producer well. Again, except for the smearing of the shock-front, the peridynamics solution captures the polymer saturation very well both behind and ahead of the shock-front.

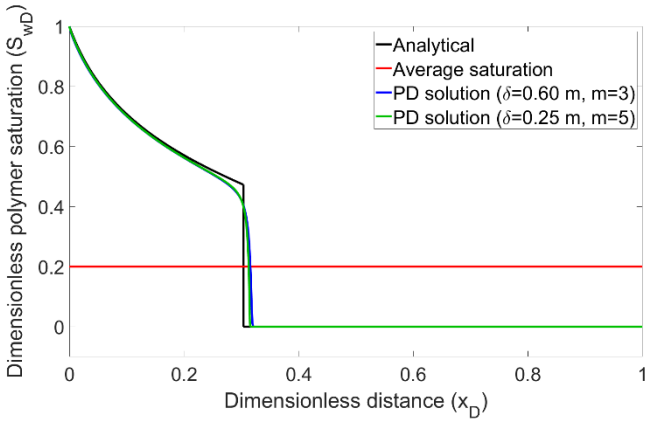

(a)

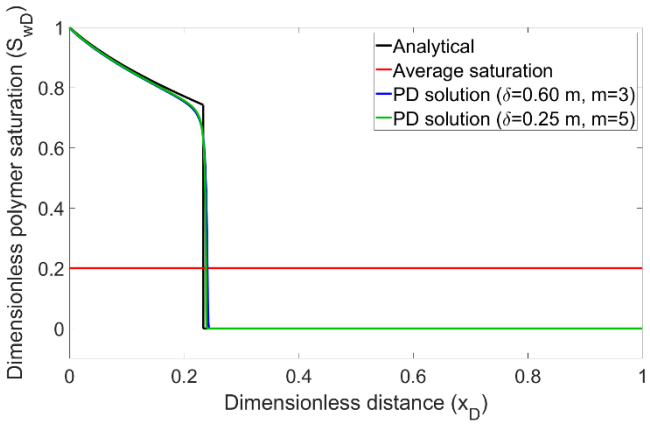

(b)

Figure 7. Analytical local and peridynamic (PD) saturation profiles before breakthrough (at t_D = 0.2) for polymer flood problem. (a): at fast injection rate (4e-5 kg/s). (b): at slow injection rate (4e-6 kg/s)

Figure 8 shows the saturation profiles for the same injection rates after the polymer solution breaks through the producer well.

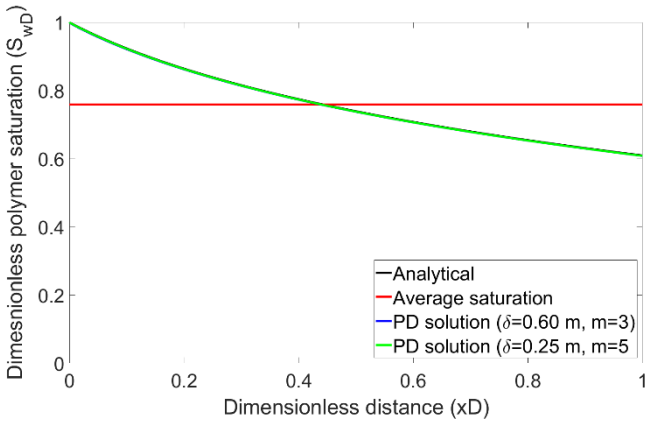

(a)

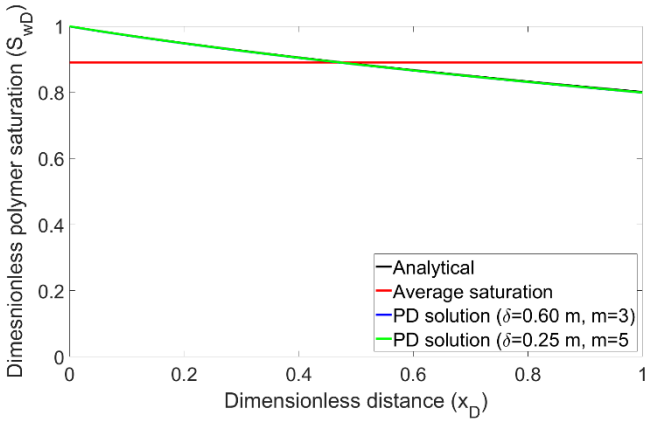

(b)

Figure 8. Analytical local and peridynamic (PD) saturation profiles after breakthrough (at t_D = 0.2) for polymer flood problem. (a): at fast injection rate (4e-5 kg/s). (b): at slow injection rate (4e-6 kg/s)

Figure 9 shows the recovery plots for the corresponding injection rates. There is an excellent match with the analytical local solution in these plots. At slower injection rate, the peridynamic simulations predict a higher oil recovery which is consistent with the findings of Wu et al. (1991).

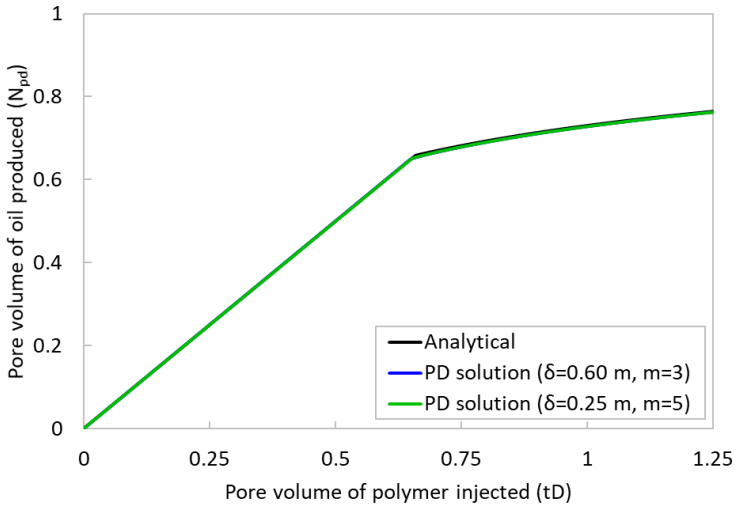

(a)

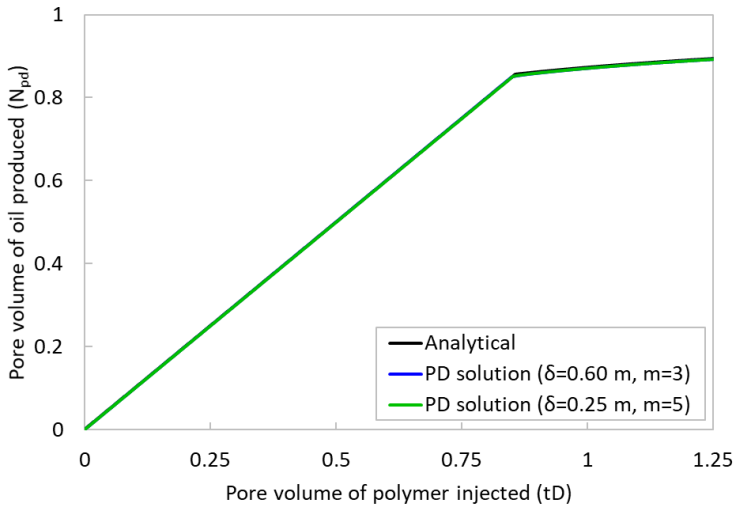

(b)

Figure 9. Analytical local and peridynamic (PD) recovery plots for polymer flood problem. (a): at fast injection rate (4e-5 kg/s). (b): at slow injection rate (4e-6 kg/s)

3.2.3. Convergence study

Following the same procedure as outlined in Section 3.1.3, Figure 10 has been obtained to show the convergence of non-local solution towards analytical local solution. The differences in this case are larger compared to those in the waterflood problem (Figure 4) because the shock-front is smeared out further. However, they are still within the acceptable range of errors for engineering applications and more accurate results can be obtained at the expense of higher computational resources.

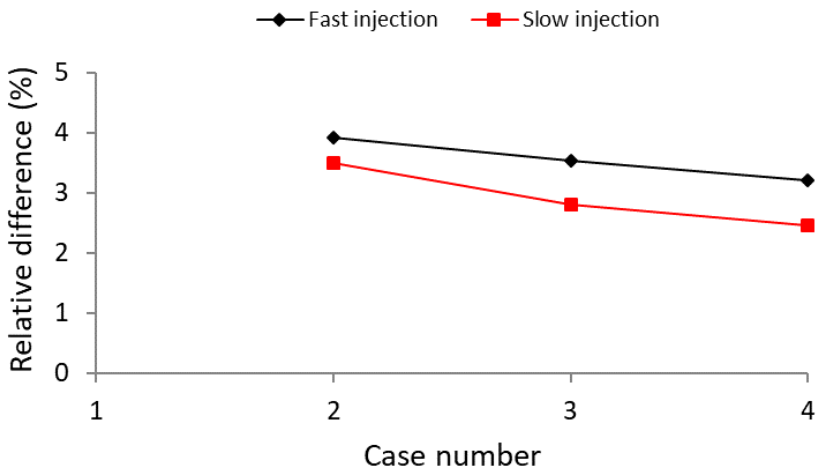

Figure 10. Relative difference in polymer saturation profile as horizon size *(δ)* decreases and number of non-local neighbors *(m)* increases simultaneously as shown in Table 2.

Figure 11 shows the relative differences in oil recovery at t_D = 0.2 PV. It should be noted that although the shock-fronts in the saturation profiles are smeared out further, the relative differences in oil recovery are negligible. This signifies that the mass conservation is honored in these simulations.

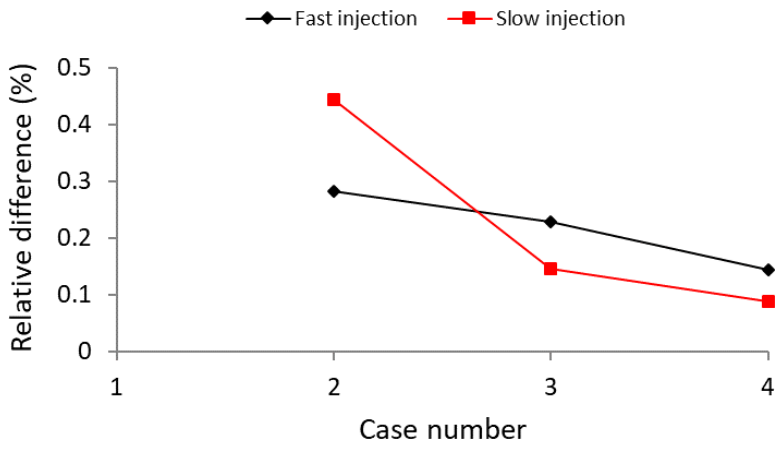

Figure 11. Relative difference in oil recovery as horizon size *(δ)* decreases and number of non-local neighbors *(m)* increases simultaneously as shown in Table 2.

3. Conclusions

In Katiyar et al. (2014), a state-based peridynamic formulation for single phase convective transport of a fluid with small, constant compressibility and Newtonian flow characteristics was presented. In this research, we have generalized the model to multi-phase, multi-component fluids showing varying compressibility and non-Newtonian behavior. These non-local fluid flow models have been derived with an intent of applying them to our peridynamics-based hydraulic fracturing simulator (Ouchi et al., 2015). Thus, we have chosen to simplify the derived equations for different kinds of multiphase models used in petroleum engineering. A compositional model is not presented because of its associated computational costs. Less expensive models such as black-oil and immiscible two-phase flow models are presented in detail.

We have demonstrated application of the multiphase model by solving 1-D linear, immiscible displacement of oil by water (water flood) and by a shear-thinning polymer (polymer flood). Saturation profiles show a characteristic shock front in such problems, which is smeared out in our peridynamic solutions due to it being a non-local formulation. A δ-m convergence study is performed to recover the analytical local solution from numerical non-local solution by shrinking the horizon size *(δ)* and increasing the number of non-local neighbors *(m)* simultaneously. Thus, saturation profiles retrieve the shock front for the two problems. Moreover, convergence of oil recovery plots to the analytical local solution verifies overall mass conservation in the proposed non-local model. In the polymer flood problem, our simulations also capture the observation that oil recovery decreases at higher injection rates of a shear-thinning polymer.

Following this research, we are currently working on validating the developed peridynamics model in higher dimensions with the laboratory-scale hydraulic fracturing experiments and field scale observations involving multiple phases. These work have been reported in separate publications (Agrawal et al., 2018; Agrawal and Sharma, 2018).

Acknowledgements

This work is supported by DOE Grant No. DE-FOA-0000724 and by the member companies participating in the Joint Industry Program on Hydraulic Fracturing and Sand Control at the University of Texas at Austin.

References

Aarnes, J.E., T. Gimse, and K.A. Lie. 2007. "An Introduction to the Numerics of Flow in Porous Media Using Matlab." Pp. 265–306 in *Geometric Modelling, Numerical Simulation, and Optimization: Applied Mathematics at SINTEF*. Springer Berlin Heidelberg.

Agrawal, S., H. Ouchi, M.J. AlTammar, and M.M. Sharma. 2018. "Mechanistic Explanation of the Impact of Pore Pressure on Hydraulic Fracture Propagation." in *52nd US Rock Mechanics / Geomechanics Symposium*.

Agrawal, S. and M.M. Sharma. 2018. "Impact of Pore Pressure Depletion on Stress Reorientation and Its Implications on the Growth of Child Well Fractures." in *6th Unconventional Resources Technology Conference*.

Bobaru, F. and M. Duangpanya. 2010. "The Peridynamic Formulation for Transient Heat Conduction." *International Journal of Heat and Mass Transfer* 53(19–20):4047–59.

Bobaru, F. and Y.D. Ha. 2011. "Adaptive Refinement and Multiscale Modeling in 2D Peridynamics." *International Journal for Multiscale Computational Engineering* 9(6):635–60.

Bobaru, F., M. Yang, L.F.Alves, S.A. Silling, E. Askari, and J. Xu. 2009. "Convergence , Adaptive Refinement , and Scaling in 1D Peridynamics." *International Journal for Numerical Methods in Engineering* (August 2008):852–77.

Brooks, R. H. and A. T. Corey. 1964. "Hydraulic Properties of Porous Media." *Hydrology Papers, Colorado State University. Fort Collins CO* 3(3):27 pgs.

Buckley, S. E. and M. C. Leverett. 1942. "Mechanism of Fluid Displacement in Sands." *Transactions of the AIME* 146: 107-116.

Chavent, G. and J. Jaffre. 1986. *Mathematical Models and Finite Elements for Reservoir Simulation*. Elsevier 17.

Chen, Z., G. Huan, and Y. Ma. 2006. *Computational Methods for Multiphase Flows in Porous Media*. Society for Industrial and Applied Mathematics.

Coats, K. H., L. K. Thomas, and R. G. Pierson. 1998. "Compositional and Black Oil Reservoir Simulation." *SPE Reservoir Evaluation & Engineering* 1(04): 372-379.

Cortis, A. and B. Berkowitz. 2004. "Anomalous Transport in 'Classical' Soil and Sand Columns." *Soil Science Society of America Journal* 68(5):1539.

Ganti, V., M.M. Meerschaert, Efi Foufoula-Georgiou, Enrica Viparelli, and Gary Parker. 2010. "Normal and Anomalous Diffusion of Gravel Tracer Particles in Rivers." *Journal of Geophysical Research* 115:1–12.

Katiyar, A., J.T. Foster, H. Ouchi, and M.M. Sharma. 2014. "A Peridynamic Formulation of Pressure Driven Convective Fluid Transport in Porous Media." *Journal of Computational Physics* 261:209–29.

Koch, D.L. and J.F. Brady. 1988. "Anomalous Diffusion in Heterogeneous Porous Media." *Physics of Fluids* 31(5):965.

Ouchi, H., A. Katiyar, J. York, J.T. Foster, and M.M. Sharma. 2015. "A Fully Coupled Porous Flow and Geomechanics Model for Fluid Driven Cracks: A Peridynamics Approach." *Computational Mechanics* 55(3):561–76.

Seleson, P.D. 2010. "Peridynamic Multiscale Models for the Mechanics of Materials: Constitutive Relations, Upscaling from Atomistic Systems, and Interface Problems."

Seleson, P.D., M. Gunzburger, and M.L. Parks. 2013. "Interface Problems in Nonlocal Diffusion and Sharp Transitions between Local and Nonlocal Domains." *Computer Methods in Applied*

Mechanics and Engineering 266:185–204.
Seleson, P.D. and M.L. Parks. 2011. “On the Role of the Influence Function in the Peridynamic Theory.” *International Journal for Multiscale Computational Engineering* 9(6):689–706.
Silling, S.A., M. Epton, O. Weckner, J. Xu, and E. Askari. 2007. *Peridynamic States and Constitutive Modeling*. Vol. 88.
Silling, S.A. 2000. “Reformulation of Elasticity Theory for Discontinuities and Long-Range Forces.” *Journal of the Mechanics and Physics of Solids* 48(1):175–209.
Wu, Y. S., K. Pruess, and P. A. Witherspoon. 1991. “Displacement of a Newtonian Fluid by a Non-Newtonian Fluid in a Porous Medium.” *Transport in Porous Media* 6(2):115–42.